

Hydrogen Bonding Versus Electrostatic Driving Forces of Phosphate Binding at the Air - Water
Interface

Research Thesis

Presented in partial fulfillment of the requirements for graduation *with research distinction* in
Chemistry in the undergraduate College of Arts and Sciences of The Ohio State University

By

Alexander Grooms

The Ohio State University

April 2019

Project Advisor:

Dr. Heather C. Allen

Department of Chemistry and Biochemistry

1 ABSTRACT

2 There is an increasing need to understand the principles of phosphate recognition.
3 Phosphate is in high demand due to fertilizer and biofuel production but supplies are limited
4 because of depleting phosphorus rock mines. Eutrophication caused by agricultural runoff leaves
5 the human phosphate cycle open and devastates aquatic ecosystems. Aqueous phosphate
6 recognition and recycling could play an important role in energy conservation, food security, and
7 water management. Phosphate recognition also has biological application in ATP and AMP
8 binding. However the principles of aqueous phosphate capture are not well understood.
9 Langmuir monolayers at the air – water interface provide a unique environment to study the
10 physical properties and chemical driving forces of phosphate binding. An amphiphilic receptor
11 with an ammonium headgroup (**U-Ammo⁺**) and a receptor with a guanidinium headgroup (**U-**
12 **Guan⁺**) were employed in this study. **U-Ammo⁺** provides pure electrostatic binding interactions
13 through the charged dimethyl ammonium headgroup, and **U-Guan⁺** provides both hydrogen
14 bonding and electrostatic interactions through the charged guanidinium headgroup. The binding
15 constants were determined for both molecules using surface sensitive infrared analysis at 5.5 °C
16 and 31.5 °C via a Langmuir-type fit. The binding constants were used with temperature in Van't
17 Hoff equations to obtain enthalpy, entropy, and free energy of phosphate binding. Overall **U-**
18 **Guan⁺** had larger binding constants and free energy driving forces than **U-Ammo⁺**, suggesting
19 **U-Guan⁺** is a better phosphate receptor. Both receptor-phosphate binding showed enthalpy as
20 the main driving force. **U-Guan⁺** showed less entropic hindrance to binding suggesting
21 preorganization. **U-Guan⁺** has previously shown selectivity up to 1:1000 phosphate-chloride
22 while in this study, **U-Ammo⁺** showed minimal phosphate selectivity at 1:1 phosphate-chloride
23 concentration.

24 **ACKNOWLEDGEMENTS:**

25 I would like to thank Jennifer Neal for the support and assistance in designing and
26 performing the experiments for this study, the editing and counseling provided in the writing of
27 this thesis, as well as continued mentorship through three years of undergraduate research. I
28 would also like to thank the Allen group for their mentorship and feedback on my project and Dr.
29 Heather Allen for presenting me with the opportunity to perform academic research in the field
30 of my choice. Lastly, I would like to thank the Department of Chemistry and Biochemistry and
31 the Undergraduate Research Office at The Ohio State University for financial and educational
32 support.

33

34 **PUBLICATIONS:**

35 Neal, J. F.; Zhao, W.; Grooms, A. J.; Flood, A. H.; Allen, H. C. Arginine-Phosphate Recognition
36 Enhanced in Phospholipid Monolayers at Aqueous Interfaces. *J. Phys. Chem. C* **2018**.

37

38 Neal, J. F.; Zhao, W.; Grooms, A. J.; Smeltzer, M. A.; Shook, B. M.; Flood, A. H.; Allen, H. C.
39 Interfacial Supramolecular Structures of Amphiphilic Receptors Drive Aqueous Phosphate
40 Recognition. *In Review*. **2019**.

41

42

43

44

45

46

47	Table of Contents	
48	Abstract.....	1
49	Chapter 1: Motivations and Background.....	5
50	1.1 Phosphate Demand.....	5
51	1.2 The Human Phosphorus Cycle and Eutrophication.....	6
52	1.3 The Principles and Challenges of Phosphate Recognition.....	7
53	1.4 Objectives.....	8
54	Chapter 2: The Air – Water Interface and Phosphate Binding.....	9
55	2.1 Benefits of Interfacial Water.....	9
56	2.2 Langmuir Monolayers and Surface Pressure – Area Isotherms.....	10
57	2.3 Infrared Reflection Absorption Spectroscopy.....	11
58	2.4 Receptor Structure and Function in Phosphate Recognition.....	12
59	2.5 A Thermodynamic Approach to Phosphate Binding.....	14
60	Chapter 3: Materials and Methods.....	16
61	3.1 Materials.....	16
62	3.2 Methods.....	17
63	Chapter 4: Results and Discussion.....	20
64	4.1 U-Ammonio ⁺ -Phosphate Interactions at the Air – Water Interface.....	20
65	4.2 U-Guan ⁺ -Phosphate Interactions at the Air – Water Interface.....	26
66	4.3 Comparison of U-Ammonio ⁺ and U-Guan ⁺ Affinity for Phosphate.....	32
67	4.4 Anion Selectivity of Receptors Between Chloride and Phosphate Anions.....	35
68	Chapter 6: Conclusions and Future Work.....	36
69	Chapter 7: References.....	38

70 CHAPTER 1: MOTIVATIONS AND BACKGROUND

71

72 1.1 Phosphate Demand

73 Phosphorus is an integral component of a growing and delicate system of water
74 management, energy conservation, and food security in modern global society.¹ Biofuel
75 production depends on the usage of phosphorus, and biofuels are increasingly important for
76 alternative energy sources.¹ However, phosphorus rock is a limited and non-renewable natural
77 resource.^{1,2} Reserves of phosphorus rock are predicted to be depleted in the next 50 to 100 years,
78 with United States supplies limited to 30 years.² In addition to these constraints, remaining
79 phosphorus rock reserves are largely located in politically and economically unstable parts of the
80 world (such as Morocco's Bou Craa mine in the Western Sahara), and therefore will take
81 increasing energy and money to mine and transport.²

82 With growing populations, there is an increasing need for higher food production. This
83 will require more efficient agricultural industries with higher crop yield per unit area of
84 cultivation.² Phosphorus, and its aqueous form phosphate, is an important constituent of modern
85 agricultural fertilizers along with nitrogen, sulfurous, and potassium.² In the context of this
86 research, the term phosphate will be used to refer to H_2PO_4^- , which is the major species present
87 in unpolluted, natural waters.³ Because phosphorus rock is limited, there is a critical need for
88 anthropogenic phosphate recycling.^{2,4} Recycling agricultural phosphate has the potential to
89 decrease the energy used in fertilizer production and increase the availability of phosphate for
90 fertilizer production, which has increasing demand with growing populations.⁴

91

92

93 1.2 The Human Phosphorus Cycle and Eutrophication

94 It is necessary to sequester and recycle phosphate used in agricultural fertilizers to
95 effectively close the human phosphorus cycle. When phosphate-based fertilizers or manure
96 applications (which are high in phosphate⁵) are used on crops, there is an excess of phosphate
97 deposited in the surface levels of the soil.^{2,5} Surface phosphate transfers to water sources via rain
98 or irrigation in a process known as agricultural runoff.^{5,6} Phosphate pollution comes from a
99 number of agricultural sources and not a single definable source, therefore it is referred to as a
100 non-point source of pollution.^{7,8} The natural phosphorus cycle cannot efficiently process the high
101 amounts placed by agriculture. When excess phosphate departs the cycle through agricultural
102 runoff and erosion, the cycle is left open.^{6,8}

103 The consequence of runoff from non-point agricultural sources is increased amounts of
104 aqueous phosphate in water sources such as ponds, lakes, rivers, deltas, and shorelines.^{7,9,10} The
105 amount and conditions of phosphate runoff vary depending on season and location, but the
106 concentration ranges from 0.1 to 0.5 mg/L which corresponds to ~10 μM .^{5,11,12} The pH
107 conditions associated with runoff conditions are between pH 4.5 to 8.^{11,12} The majority of this
108 range corresponds to the H_2PO_4^- speciation of aqueous phosphate, which was employed within
109 this study.^{3,13}

110 Excess amounts of phosphate induce a phenomenon known as eutrophication in which
111 large amounts of aquatic algae grow and coat the water's surface.⁸⁻¹⁰ Phosphate is the limiting
112 factor in eutrophication, as this nutrient promotes the growth of biologically simple algae over
113 more complex aquatic plant life.^{9,10} When algal blooms progress and begin to die, the
114 decomposition of the bloom depletes aqueous oxygen via cellular respiration.^{7,9,10,14} The lowered
115 oxygen levels in the waters causes the death of other aquatic life, leading to areas known as

116 “dead zones” where the ecosystem has been decimated.^{7,9,10} As a result, there is a heightened
117 need to reduce anthropogenic phosphate pollution. This ecosystem remediation would result in
118 cleaner water supplies for drinking, and less economic and energetic strain in cleaning/aiding
119 areas affected by algal blooms and dead zones.^{9,10,15}

120

121 **1.3 The Principles and Challenges of Phosphate Recognition**

122 The need for anthropogenic phosphate remediation is complimented by the continued
123 need to better understand the physical-organic principles behind phosphate recognition.¹⁵

124 Phosphate binding can occur through two fundamental intermolecular interactions. Electrostatic
125 interactions may occur between the negative charge on phosphate and a positive charge on a
126 receptor. Also, hydrogen bonding may occur between the O-H groups on the phosphate and a
127 complementary hydrogen bond acceptor/donor. Both of these interactions have been shown as
128 important factors for strong, selective binding phosphate over other anions in solution.¹⁶⁻¹⁸

129 Selective phosphate binding in an aqueous environment comes with the challenge of a
130 large energetic penalty for phosphate dehydration, which has a ΔG_{hyd} of -465 kJ/mol.¹⁹ Another
131 complication interfering with binding between a phosphate guest and receptor host is the large
132 dielectric constant (ϵ) of bulk water ($\epsilon = 80$).^{3,20,21} The dielectric constant is an important factor
133 in intermolecular binding interactions because it is the quantity by which Coulombic force
134 between charges are shielded. A higher dielectric constant corresponds to more Coulombic
135 shielding between positive and negative charges and therefore less effective interactions.^{21,22}
136 Phosphate also has a large size to charge ratio that is resultant of the singular negative charge
137 delocalized over the large phosphate molecule.^{3,20} One last complication in phosphate binding is
138 the acid/base qualities of triprotic phosphate, resulting in multiple possible species of phosphate

139 in solution depending on the pH.^{3,13} The pK_a's of phosphate are pK_{a1} = 2.16, pK_{a2} = 7.21, and
140 pK_{a3} = 12.32.²³

141 There is a literature precedence of using guanidinium receptors in low dielectric constant
142 environments provided by organic solvents, such as DMSO for the recognition of
143 phosphate.^{16,24-28} A specific technique that has recently been investigated is the guest-host
144 interactions of phosphate-guanidinium at the air-water interface, which benefits from a
145 decreased dielectric environment^{18,21}. This technique will be subsequently discussed in more
146 detail. A principle of phosphate recognition that has not been extensively studied is the
147 thermodynamic driving forces behind the binding process.

148

149 **1.4 Objectives**

150 A primary goal for this project is to compare the driving forces for phosphate binding to
151 amphiphilic receptors at the air – water interface. The guest-host intermolecular interactions that
152 occur between negatively charged phosphate, a positively charged receptor, and a positively
153 charged receptor with hydrogen bond donors will be understood. This will be evaluated at the
154 air - water interface due to the decreased dielectric constant present at the interface.^{21,22} It will
155 be determined qualitatively whether hydrogen bond-assisted electrostatic interactions between
156 guest and host are more effective than pure electrostatic binding. Furthermore, an investigation
157 of whether a hydrogen bond-assisted electrostatic binding receptor will provide phosphate
158 selectivity over a pure electrostatic binding receptor. Lastly, the binding coefficients between
159 host-guest association will be quantified along with enthalpy of binding (ΔH°), entropy of
160 binding (ΔS°), and free energy of binding (ΔG°). The specific theory and technique that will be
161 employed to meet these objectives will be discussed in Chapter 2.

162
163
164
165
166
167
168
169
170
171
172
173
174
175
176
177
178
179
180
181
182
183
184

CHAPTER 2: THE AIR – WATER INTERFACE AND PHOSPHATE BINDING

2.1 Benefits of Interfacial Water

The large ϵ of bulk water suggests that significant charge shielding occurs.^{3,20} The lessening of positive and negative electrostatic interaction along with positive and negative dipole interaction found in hydrogen bonding is what makes water an excellent solvent, however it also greatly inhibits host-guest binding.^{21,22,29} The high ϵ of bulk water has been attributed to the large degree of rotational freedom that the molecules possess in unconfined space.²¹ The ability for water dipoles to rotate freely suggests that bulk water has high electric polarizability – or has the potential to reorient dipoles in the presence of an electric field. Charges and partial charges on molecules in aqueous solution act as small electric fields - thus free-rotating bulk water molecules may align around the field forming a solvation shell, solvating the charged molecule, and preventing it from firmly binding to another charged species in solution.^{29,30}

A recent experimental study has given support to theoretical studies that the ϵ of water greatly decreases at interfaces.²¹ When water molecules are confined near an interface they lose a large degree of rotational freedom and align dipoles at the surface, which results in a decrease of the ability to align in an electric field.^{31–33} Decreased polarizability suggests that interfacial water does not act to shield charges as much as bulk water. Consequently, the magnitude of the dielectric constant depended greatly on the thickness of the confined water layers ranging from $\epsilon = 2$ in the thinnest layers to $\epsilon \sim 20$ at thicker interfacial water.²¹ An additional study indicates that electrostatics govern the affinity between anions and cations in solvents with low dielectric

185 constants.³⁰ These previous findings are important in the context of this study because the low
186 dielectric constant of surface water at the air – water interface will be taken advantage of, along
187 with the amphiphilic design of positively charged receptors, to sequester and bind negatively
188 charged phosphate at the surface.

189

190 **2.2 Langmuir Monolayers and Surface Pressure – Area Isotherms**

191 A Langmuir monolayer describes the two dimensional environment when a thin film is
192 spread over the surface of water. These films are often comprised of amphiphilic molecules with
193 long, hydrophobic, alkyl chains and a hydrophilic headgroup. These molecules orient at the air –
194 water interface with the hydrophobic tails pointing away from the water and the hydrophilic
195 headgroup interacting with the surface layers of water. Langmuir monolayers provide multiple
196 benefits that lead to improved binding at the air – water interface. First, monolayers have been
197 utilized because of their self-organization and confined micro-environment.^{34,35} The pre-
198 organized environment of self-aligning molecules at the surface of water allow for optimization
199 of the molecular design – improving the molecule’s performance in binding.^{35,36} A benefit
200 realized from the preorganization of Langmuir monolayers is an enthalpically favorable binding
201 region.^{36,37} The preorganization of the monolayer means that less energy is needed to place the
202 guest and the host into the proper orientation for binding. Multiple studies have taken advantage
203 of these benefits to investigate the binding of guests to the monolayer hosts.^{38–41}

204 Surface Pressure – Area (Π -A) Isotherms are an analytical technique utilized in the study
205 of Langmuir monolayers. Π -A isotherms measure the Π of a monolayer film as a function of
206 mean-molecular area. The underlying physical principle behind the isotherm is that as the mean
207 molecular area between amphiphilic molecules oriented at the surface of water decreases, the

208 surface pressure will increase, which packs the long hydrophobic tails in closer proximity. The
209 molecules are spread onto the surface of water in what is known as the gaseous phase. This
210 occurs at high mean molecular areas, where there is a low degree of hydrophobic tail
211 organization, loose molecular packing, and low surface pressure. When the molecules are
212 compressed to a specific mean molecular area, they enter the condensed phase in which the
213 molecules begin to attain order, and the tails are not as free as in the gas phase. Lastly, at low
214 mean molecular area, the molecules enter the collapse phase in which the tails are well ordered
215 and packed closely together. In previous studies, Π -A isotherms have been used to observe
216 binding events by monitoring the expansion in mean molecular area at a given surface pressure,
217 which arises due to differing monolayer ordering/organization between bound and unbound
218 states.^{18,42-44} One of the amphiphiles used in this study was adopted from Neal *et. al.* The design
219 of this receptor will be discussed later, but it is important to note that this molecule showed no
220 mean molecular area expansion which was attributed to the long alkyl chains masking any
221 monolayer re-ordering due to binding.

222

223 **2.3 Infrared Reflection Absorption Spectroscopy**

224 Infrared Reflection Absorption Spectroscopy (IRRAS) is a useful method to investigate
225 structural information and understand binding affinities at the air – water interface. This
226 technique brings the advantages of infrared spectroscopy to the surface of water, allowing the
227 identification of functional groups in molecules at the surface. Infrared light perturbs molecular
228 vibrations that result in an oscillating dipole moment, which is characteristic of specific types of
229 vibrations in a bond between atoms.⁴⁵

230 A typical IRRAS setup will have an infrared beam reflected from a mirror and onto the
231 surface of a Langmuir monolayer, then back to a mirror and into the detector. Data from IRRAS
232 is reported as reflectance-absorbance (RA) versus wavenumber, where RA is defined by the
233 following equation.

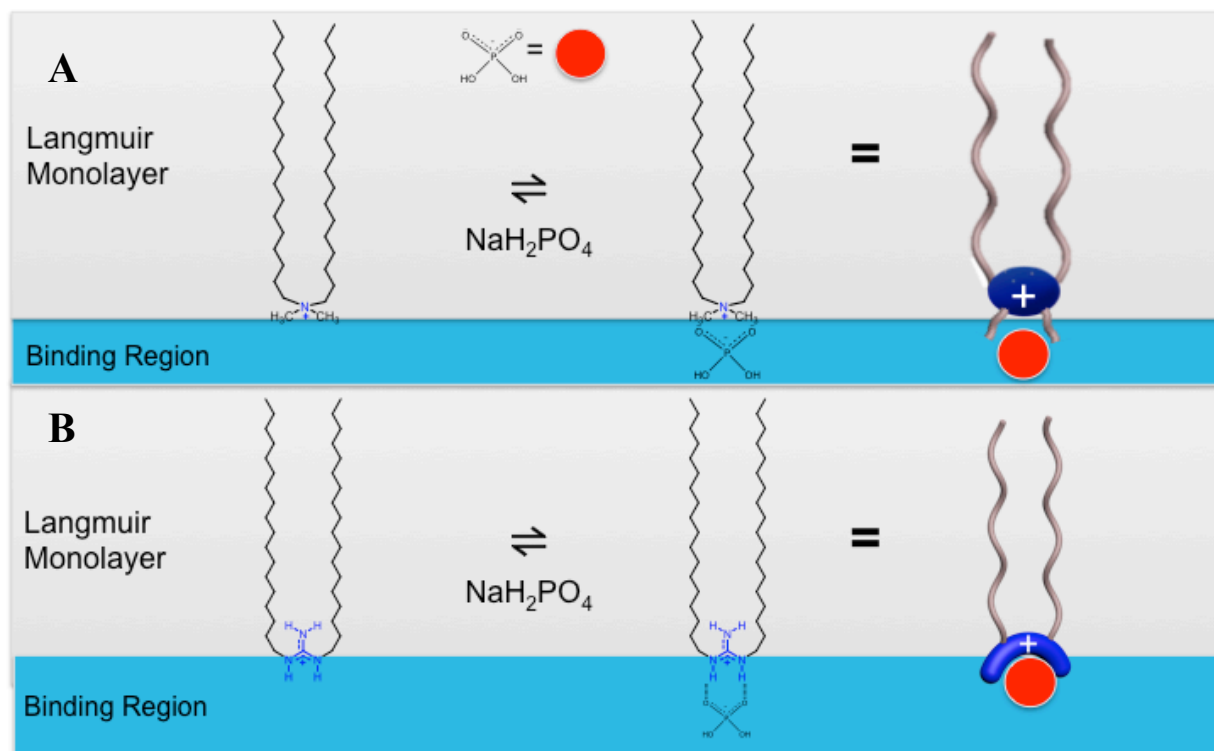
$$234 \quad RA = -\log_{10}\left(\frac{R}{R_0}\right) \quad (1)$$

235 Where R is the reflectivity of the surface of water with the Langmuir monolayer on top of it, and
236 R_0 is the reflectivity of pure water.

237 Phosphate containing compounds have been extensively studied via IRRAS and have
238 yielded well-defined characteristic frequencies of phosphate vibrations.^{35,45-48} Two modes of
239 high interest in this study are the phosphate PO_2^- asymmetric stretch that occurs $\sim 1220\text{-}1250\text{ cm}^{-1}$
240 ¹ and the phosphate PO_2^- symmetric stretch that occurs $\sim 1090\text{ cm}^{-1}$.^{45,48} Additionally, it has been
241 observed that the PO_2^- symmetric stretch can be shifted to higher frequency (blue-shifted)
242 depending on the degree of dehydration of phosphate.⁴⁹ In previous studies by Neal *et. al*, the
243 presence of PO_2^- symmetric and asymmetric stretching frequencies have been observed to
244 change based on the concentration of aqueous phosphate, suggesting binding between phosphate
245 moieties and guanidinium moieties at the air – water interface¹⁸ (in review).

246

247 **2.4 Receptor Structure and Function in Phosphate Recognition**



248

249 **Figure 1: Proposed binding motif at the air – water interface for U-Ammonium⁺-phosphate**
 250 **binding (A) and U-Guanidinium⁺-phosphate binding (B)**

251 The amphiphilic receptors in this study were chosen based on the unique intermolecular
 252 driving forces for binding that each receptor offers at the air – water interface. The receptor in
 253 **figure 1A**, dimethyldioctadecylammonium bromide (**U-Ammonium⁺**), was chosen due to the pure
 254 electrostatics at the ammonium head group and the double octadecyl alkyl chain for monolayer
 255 formation. The interactions of the **U-Ammonium⁺** molecule with phosphate are purely electrostatic
 256 due to the lack of hydrogen bond donor sites at the ammonium head group – therefore, the only
 257 interaction that may occur is between the negatively charged phosphate molecule and the
 258 positively charged ammonium.

259 The receptor in **figure 1B**, cationic dioctadecylguanidinium (**U-Guanidinium⁺**), was designed
 260 by Neal *et al* (in review) and chosen for the molecule's unique ability of the guanidinium head
 261 group to interact with phosphate via electrostatics and hydrogen bonding. There is a large

262 literature precedent for the binding of guanidinium to phosphate, which include the biological
263 inspiration of ATP and AMP binding to guanidinium functional groups.^{24,28,38,50–53} This
264 interaction has been considered successful due to the electrostatic attraction between negatively
265 charged phosphate and positively charged guanidinium, and the hydrogen bond donors on
266 guanidinium interacting with the hydrogen bond acceptors on phosphate. The ability for
267 phosphate and guanidinium to interact via hydrogen bonding in addition to electrostatics
268 suggests that phosphate should selectively bind to the **U-Guan**⁺ receptor over the **U-Ammono**⁺
269 receptor. The thermodynamic driving forces behind the binding of phosphate to a receptor at the
270 air – water interface are not well understood. Furthermore, the effect of hydrogen bond-assisted
271 electrostatic binding versus pure electrostatic binding at the air – water interface has not been
272 investigated.

273

274 **2.5 A Thermodynamic Approach to Phosphate – Receptor Binding**

275 As stated, the thermodynamic driving forces of interfacial phosphate binding are largely
276 unexplored, however the energetics of binding to a guanidinium host in bulk water, organic
277 solvent sub-phase, and at the solid – liquid interface can be applied to determine useful
278 thermodynamic quantities.^{54–57} Changes in free energy of binding (ΔG_b), enthalpy of binding
279 (ΔH_b), and entropy of binding (ΔS_b) can give detailed information about driving forces behind
280 phosphate binding and quantitative support to the proposed binding models for the **U-Ammono**⁺
281 and **U-Guan**⁺ receptors. It may be determined whether hydrogen bond-assisted electrostatic
282 binding results in a more spontaneous binding event than pure electrostatic driven binding, and
283 which thermodynamic component (enthalpy or entropy) is the principle driving force.

284 A bulk study of phosphate binding to guanidinium and ammonium host in water
285 depended largely on the solvent shell of the complex.⁵⁴ Binding to the ammonium host was
286 driven by entropy change due to the release of the solvation shell upon binding – overcoming
287 unfavorable (endothermic) enthalpy change, and binding to the guanidinium host was driven by
288 (exothermic) enthalpy change due to the pre-organized structure of the guanidinium host.⁵⁴ This
289 pre-organization in conjunction with a less hydrated environment caused the guanidinium guest
290 and phosphate host to be in a favorable binding pocket, and therefore binding occurred with
291 enthalpy as the driving force.⁵⁴ This result can be compared to the pre-organized and confined
292 setting of a Langmuir monolayer at the air – water interface providing a favorable environment
293 for enthalpy driven binding.^{36,37} Another study found that receptors capable of forming bi-
294 dentate hydrogen bonds with hosts demonstrated exothermic binding and favorable entropy
295 change.⁵⁵ This study was performed in DMSO with a lower dielectric constant ($\epsilon \sim 40$), which is
296 comparable to the significantly decreased dielectric constant at the surface of water, thus
297 amplifying phosphate binding via increased electrostatic interactions.^{21,22}

298 In order to determine the thermodynamic quantities of phosphate binding to U-Ammon+
299 and U-Guan+ receptors, the binding constant must first be determined at a series of temperatures.
300 The association binding coefficient, K_a will be obtained using the general Langmuir model in
301 **equation 2** and the assumption that the phosphate to receptor binding occurs at a 1:1 ratio. This
302 assumption has been previously made due to the nature of the binding ‘pocket’ created by the
303 hydrogen bond donors of the **U-Guan⁺** receptor (**figure 1B**).

$$304 \quad I = I_{max} \frac{[phosphate]}{(1/K_a) + [phosphate]} \quad (2)$$

305 In this equation, I is the intensity of the asymmetric PO_2^- stretching frequency after water
306 intensity subtraction and I_{max} is the maximum intensity of the stretching frequency. K_a is the

307 association binding constant. A larger K_a correlates to a stronger guest-host bind. K_a may be
308 related to ΔG_b at a specific temperature via the following thermodynamic principle where R is
309 the gas constant (8.314 J/K mol).⁵⁷⁻⁵⁹

$$310 \quad \Delta G_{b,T} = -RT \ln K_a \quad (3)$$

311 **Equation 3** may be rearranged to form **equation 4** using **equation 5** to obtain the Van't Hoff
312 equation of a line. Through Van't Hoff plots the natural log of the binding coefficient can be
313 displayed as a function of inverse temperature in **equation 4** where ΔH_b is in J/mol and ΔS_b is in
314 J/mol K.⁵⁷⁻⁵⁹

$$315 \quad \ln K_a = -\frac{\Delta H_b}{RT} + \frac{\Delta S_b}{R} \quad (4)$$

$$316 \quad \Delta G_b = \Delta H_b - T\Delta S_b \quad (5)$$

317 The values for ΔH_b can be obtained from the slope of the Van't Hoff line ($-\Delta H_b/RT$) and ΔS_b can
318 be obtained from the y-intercept of the Van't Hoff line ($\Delta S_b/R$) in the plot of $\ln K_d$ versus $1/T$.
319 The value of Gibbs free energy change at a given temperature $\Delta G_{b,T}$ may be obtained by
320 inserting ΔH_b and ΔS_b into **equation 5**, the principle equation of thermodynamics.⁵⁷

321

322

323 **CHAPTER 3: MATERIALS AND METHODS**

324

325 **3.1 Materials**

326 The materials used in this study were purchased with the exception the **U-Guan**⁺
327 receptor. This receptor was designed and synthesized in conjunction with Indiana University
328 (Wei Zhao). Multiple stock solutions of **U-Guan**⁺ stock solution were made in a 4:1 mixture of
329 chloroform:methanol (HPLC grade, Fisher Scientific). Multiple stock solutions of

330 dimethyloctadecylammonium bromide (U-Ammo⁺) (>99%, Acros Organics) were made in
331 chloroform (HPLC grade, Fisher Scientific). Sodium dihydrogen phosphate monobasic
332 monohydrate ($\geq 99.5\%$, Sigma) and sodium chloride (ACS grade Fisher, baked at 650 °C for > 8
333 hours prior to use) was dissolved in ultra pure water that had a resistivity of 18.2 M Ω cm (A10
334 Advantage) to form varying concentrations of stock phosphate solutions. The pH of the highest
335 concentration phosphate solution was 5.185.

336

337 **3.2 Methods**

338 *3.2.1 Surface Pressure – Area Isotherms*

339 Although Π -A isotherms were not used in the determination of phosphate binding
340 coefficients, the technique was necessary in IRRAS and useful for the concentration calibration
341 of the **U-Ammo⁺** and **U-Guan⁺** receptor solutions. Π -A isotherms were completed on a
342 customized Teflon Langmuir trough, which had an area of 144.5 cm² and movable Delrin
343 compression barriers (KSV NIMA, Finland). The cleaning procedure for the trough and the
344 barriers was rigorous in order to avoid contamination from which surface sensitive techniques
345 are prone. To ensure cleanliness for each trial, a quick compression of the subphase in the trough
346 was performed before each trial and the Π did not rise above 0.2 mN/m suggesting that there was
347 no surfactant contamination.

348 For the collection of Π -A isotherms, surface pressure was monitored using the Wilhelmy
349 plate method with custom cut filter paper plates (Ashless grade, Whatman). These plates were
350 soaked in ultrapure water for one minute before being placed on the surface tensiometer. KSV
351 software (KSV, Finland) controlled the surface pressure, and receptor monolayers were spread
352 drop-wise onto the aqueous surface in the trough using a microsyringe (Hamilton). The syringe

353 was cleaned thoroughly with reagent alcohol, allowed to air dry, and then cleaned ten times with
354 chloroform (HPLC grade, Fisher). Ten minutes elapsed before the start of each trial to allow for
355 solvent evaporation of the receptor spread solution. The barriers were compressed at a constant
356 speed of 5 mm/min for each barrier. When the surface pressure was reached (40 mN/m) the
357 barriers were oscillated at 1 mm/min in order to maintain constant Π .
358



359
360 **Figure 2: Experimental setup with Langmuir trough, barriers, Wilhelmy plate, and**
361 **temperature probe in the FTIR with an IRRAS mirror setup**

362

363 *3.2.2 Infrared Reflection Absorption Spectroscopy*

364 IRRAS was the principle technique used in this study to obtain phosphate-binding data. A
365 Fourier transform infrared (FTIR) spectrometer (Spectrum 100, PerkinElmer) was used to collect
366 all spectra. This FTIR had a liquid nitrogen cooled HgCdTe (MCT) detector that was filled prior
367 to each experiment. The Langmuir II-A setup was placed on a breadboard that also had two
368 gold-plated mirrors – each of which were precisely set in order to collect reflectivity of IR light
369 off of the monolayer surface at a 46 ° angle of incidence.

370 The Langmuir II-A setup was also connected to a Julabo MC temperature control system
371 (Julabo Labortechnik, Germany). Rubber tubing pumped heated or cooled water through the
372 interior of the trough, placing the sub-phase and monolayer at a desired temperature. For this
373 study, experimental temperatures were maintained at 5.5°C and 31.5 °C. The temperature
374 controller was set at 1 °C and 37 °C to obtain these temperatures, which were measured with a
375 temperature probe through the software that was placed into the sub-phase and secured to the
376 FTIR. To avoid contamination, the probe was cleaned thoroughly with reagent alcohol after
377 every trial and allowed to dry completely.

378 IRRAS background spectra were collected off of the sub-phase substance with no
379 monolayer and off of the surface of the monolayer at 40 mN/m for each trial. All spectra were
380 performed immediately after the surface pressure reached 40 mN/m for consistency and to
381 prevent any relaxation that may occur over time. IRRAS spectra were recorded by averaging 300
382 scans, which were collected using unpolarized light and the single-beam mode of the FTIR. The
383 spectra were plotted as reflectance-absorbance (RA), which was given by **equation 1**, versus
384 frequency. Data analysis was performed using Origin software (OriginLab 9, Northampton,
385 MA). Each spectrum shown represents the average of three identical experiments.

386

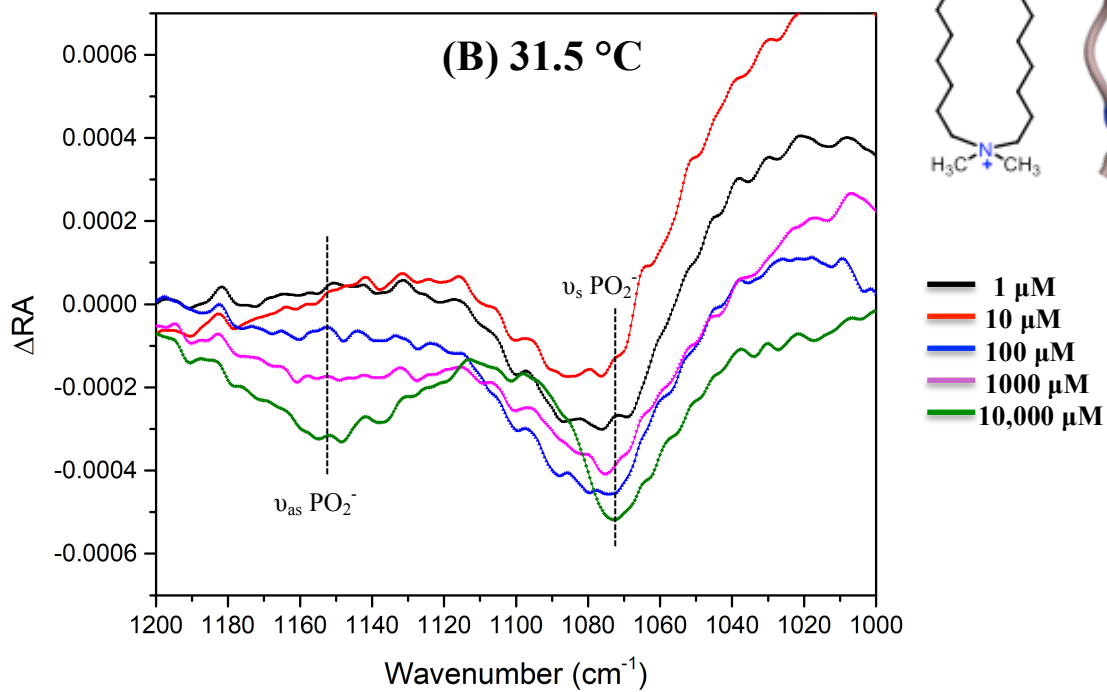
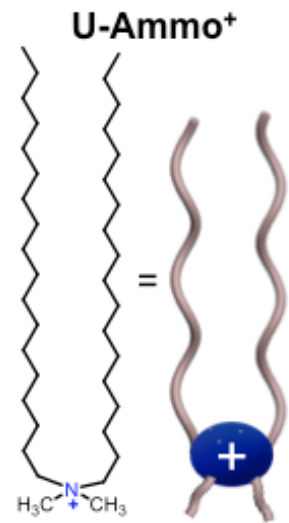
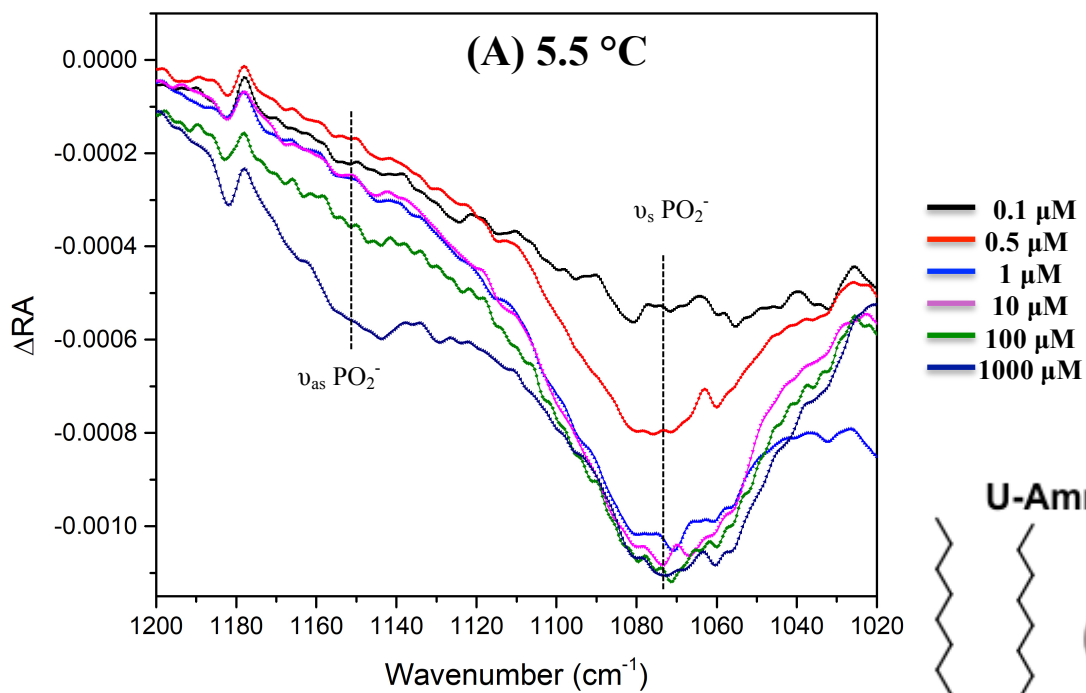
387

388 **CHAPTER 4: RESULTS AND DISCUSSION**

389

390 **4.1 U-Ammo⁺-Phosphate Interactions at the Air – Water Interface**

391 *4.1.1 U-Ammo⁺ Receptor IRRAS*



392

393
394

Figure 3: IRRAS spectra of U-Ammonium⁺ on phosphate at 5.5 °C (A) and 31.5 °C (B)

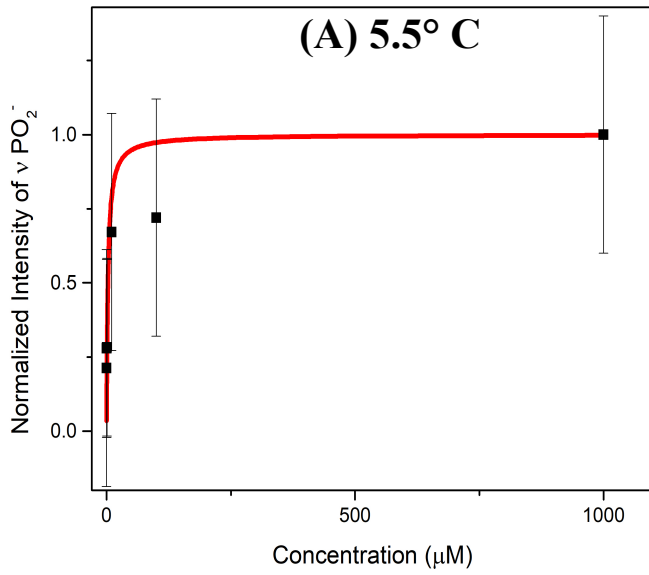
395

396 A principle goal of this project was to observe and quantify binding between the
397 receptor's head group guest and aqueous H_2PO_4^- host at different temperatures. The coupling of
398 IRRAS and temperature control allowed for spectroscopic exploration of these binding
399 interactions at 5.5 °C and 31.5 °C (**Figure 3**). These IRRAS spectra were collected at a Π of 40
400 mN/m, which corresponded, to the well-organized condensed phase of the receptor monolayer.
401 The phosphate PO_2^- stretching frequency has been shown as a binding-sensitive region.⁶⁰ This is
402 supported here where the PO_2^- symmetric stretch and the PO_2^- asymmetric stretch, which have
403 been assigned at 1071 cm^{-1} and 1150 cm^{-1} respectively^{61,62}, increase in relative intensity with
404 increasing phosphate concentration. If no phosphate-receptor binding was present then the
405 phosphate modes would not appear via IRRAS due to the nature of the reflectance-absorbance
406 equation. In this equation, the IRRAS spectrum of the receptor monolayer on phosphate sub-
407 phase is divided by spectrum of the phosphate sub-phase - thus acting to normalize any free
408 aqueous phosphate modes. The presence of these modes suggests that phosphate is being
409 attracted to the receptor monolayer at the surface of water. The spectra in **Figure 3** have also had
410 the spectra of the receptor on pure water subtracted in order to emphasize the phosphate binding
411 peaks.

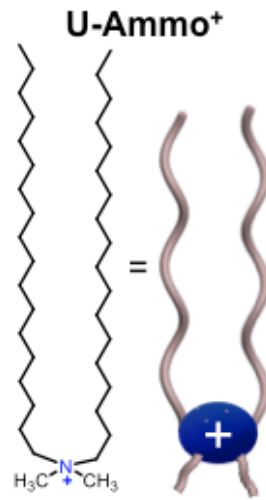
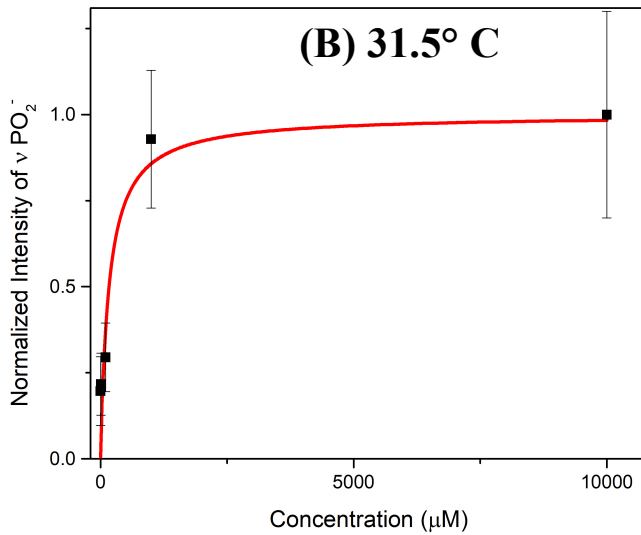
412 The 10,000 μM phosphate spectra in **Figure 3A** (dark blue) at 5.5 °C shows the PO_2^-
413 symmetric mode with a peak height of $\sim 0.0008 \Delta\text{RA}$ and a peak width of $\sim 100 \text{ cm}^{-1}$. The 10,000
414 μM phosphate spectra in **Figure 3B** (green) at 31.5 °C shows the same mode with a peak height
415 of $\sim 0.0004 \Delta\text{RA}$ and peak width of $\sim 110 \text{ cm}^{-1}$. This decrease in intensity and broadening of the
416 peak is a temperature effect that is in accordance with a Boltzmann distribution. At a higher
417 temperature, more vibrational microstates are being probed due to a higher energy system.

418

419 4.1.2 *U-Ammo*⁺ Receptor Binding Affinity



420



421

422 **Figure 4: U-Ammo⁺-phosphate normalized PO₂⁻ stretch at 5.5 °C (A) and 31.5 °C (B)**

423 **showing an increase in intensity with phosphate addition until binding site saturation.**

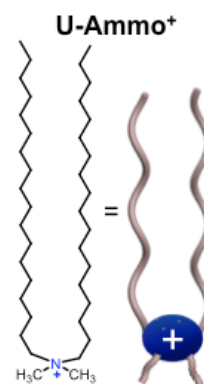
424

425 **U-Ammo**⁺-phosphate binding at 5.5 °C and 31.5 °C was quantified by plotting the
426 normalized intensity of the full PO₂⁻ stretch versus concentration of phosphate (**Figure 4**). The
427 lower temperature was integrated from 1019 cm⁻¹ to 1200 cm⁻¹ and the high temperature was
428 integrated from of 992 cm⁻¹ to 1200 cm⁻¹ in order to account for the peak broadening observed at
429 the higher temperature. The peak integration of pure water was subtracted from each of the
430 phosphate concentrations and was then normalized by dividing by the maximum peak intensity.
431 Due to this normalization, “0” represents the intensity of **U-Ammo**⁺ on water and “1” represents
432 the highest PO₂⁻ intensity in the probed region. This data was then fit to the general Langmuir
433 model (equation 2) to quantify K_a and plotted to obtain the binding curves. The error bars in
434 **figure 4** represent the propagated error of the standard deviation of three identical trial
435 integrations, subtraction of water intensity, and normalization division. **Figure 4A** shows the
436 Langmuir fit of **U-Ammo**⁺ binding to phosphate at 5.5 °C, which yielded a binding affinity of K_a
437 = 3.62×10⁵ ± 2×10⁵ M⁻¹. The Langmuir fit of **U-Ammo**⁺-phosphate binding at 31.5 °C seen in
438 **figure 4B** gave a binding affinity of K_a = 5.9×10³ ± 3×10³ M⁻¹. This decrease in magnitude
439 suggests that the **U-Ammo**⁺ receptor becomes significantly worse at binding to phosphate at
440 higher temperatures. Additionally, a larger K_a at low temperatures suggests that enthalpy is the
441 principle driving force of binding – with binding being less favorable at higher temperature,
442 more energetic environments.

443

444 *4.1.3 Thermodynamic Driving Forces of U-Ammo*⁺*-phosphate Binding*

T	K (M ⁻¹)	1/T	ln K	error
278.5 K	3.62×10 ⁵	0.00359	12.799	±0.54
304.5 K	5.9×10 ³	0.00328	8.683	±0.50

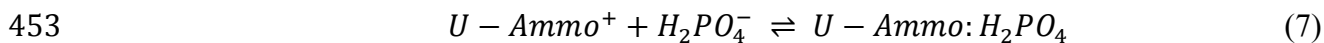


445

446 **Figure 5: U-Ammo⁺ Van't Hoff data from which the ΔH°_b and the ΔS°_b were respectively**
 447 **obtained.**

448

449 The thermodynamic driving forces of U-Ammo⁺ binding to phosphate may be quantified
 450 via Van't Hoff analysis (**figure 5**), in which the two points may approximate the slope of the
 451 line. The K_a obtained from the Langmuir fit, assuming 1:1 phosphate-receptor binding, may be
 452 visualized as a binding equilibrium constant between bound and unbound states (equation 7,8).



454
$$K_a = \frac{(U Ammo:H_2PO_4)}{(U Ammo^+)(H_2PO_4^{2-})} \quad (8)$$

455 Where K_a may be used to obtain ΔH_b , ΔS_b , and $\Delta G_{b,T}$ through the Van't Hoff equation
 456 (equations 2-6).⁵⁷⁻⁵⁹ A summary of thermodynamic quantities may be seen in **Table 1**.

457

458

U-Ammo⁺					
K_{a,5.5° C} (M⁻¹)	K_{a,31.5° C} (M⁻¹)	ΔH_b (J/mol)	ΔS_b (J/mol K)	ΔG_{5.5° C} (J/mol)	ΔG_{31.5° C} (J/mol)
3.62×10 ⁵	5.9×10 ³	-1621	-4.27	-429.2	-318.2

459 **Table 1: Thermodynamic values for U-Ammo⁺-phosphate binding**

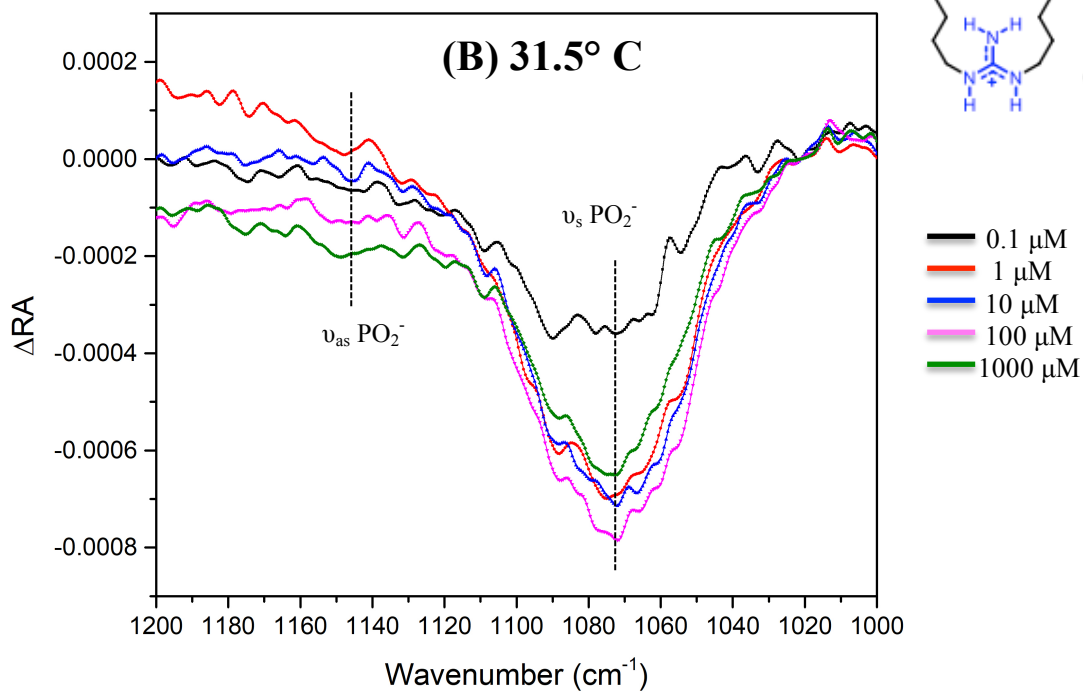
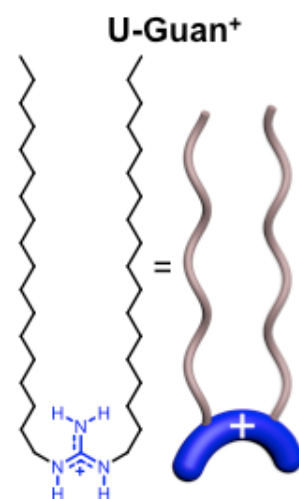
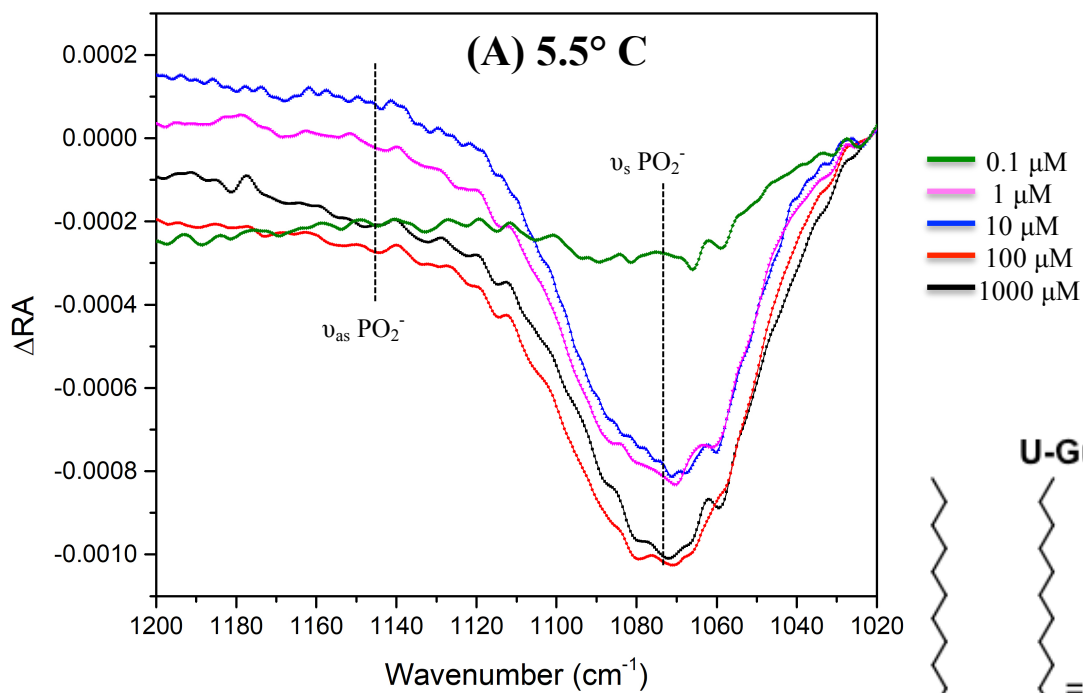
460

461 The negative ΔH_b and negative ΔS_b of U-Ammo⁺ binding to phosphate suggests that this binding
462 process is enthalpically driven rather than entropically driven. The negative ΔS_b may be
463 explained in the context of this binding environment because the un-bound system yields more
464 microstates, where as the bound system is more ordered with fewer microstates. Upon binding
465 the system become more organized overall and therefore causes an unfavorable negative entropy
466 change. The expected enthalpic driving force is a product of the benefits of Langmuir
467 monolayers at the air-water interface creating a low ε environment in which electrostatic
468 interactions dominate anion binding.^{30,36,37} The negative ΔG_b at both high and low temperature
469 display that receptor-phosphate binding is spontaneous, but more so at the lower temperature,
470 which is another product of enthalpy driven binding. It should be noted that a third data point
471 will be obtained at 15 °C in order to confirm the Van't Hoff analysis used herein.

472

473 **4.2 U-Guan⁺-Phosphate Interactions at the Air – Water Interface**

474 *4.2.1 U-Guan⁺ Receptor IRRAS*



475

476
477

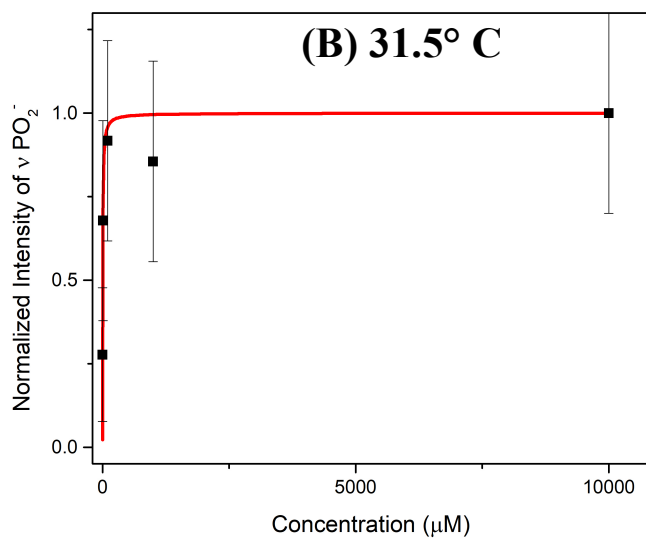
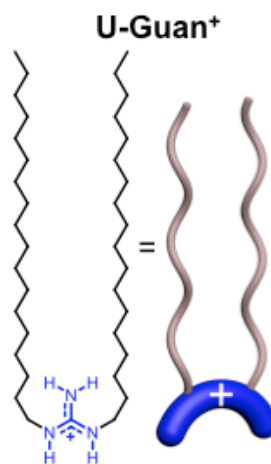
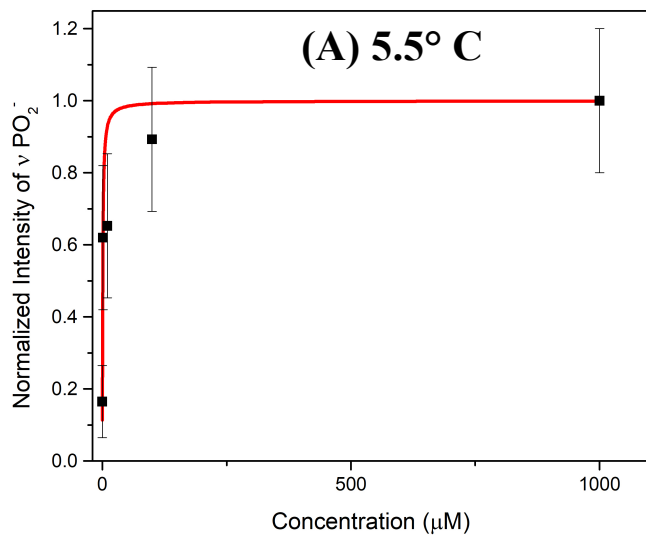
Figure 6: IRRAS spectra of U-Guan⁺ on phosphate at 5.5 °C (A) and 31.5 °C (B)

478

479 IRRAS spectra of the **U-Guan**⁺ receptor at 5.5 °C and 31.5 °C on a range of phosphate
480 concentration sub-phases were utilized to determine **U-Guan**⁺-phosphate binding in the same
481 manner as discussed for the **U-Ammono**⁺ receptor (**figure 6**). These spectra have again had the
482 water spectrum subtracted from each phosphate spectrum and are therefore plotted as ΔRA
483 versus wavenumber. The PO_2^- symmetric stretch again occurs at 1071 cm^{-1} and varies with
484 phosphate concentration. It is seen that at high concentrations the binding of phosphate to **U-**
485 **Guan**⁺ becomes saturated, as the PO_2^- symmetric stretch of the 1 μM phosphate solution has
486 similar relative intensity to the 10,000 μM solution for both low and high temperatures. These
487 similar intensities suggest that the number of binding sites quenched at a low sub-phase
488 phosphate concentration, which could be attributed to the hydrogen bond-assisted electrostatic
489 interactions between the guanidinium head group and $H_2PO_4^-$. The temperature effect on the
490 infrared peaks is again observed as a broadening of the PO_2^- symmetric stretch from 5.5 °C
491 (**figure 6A**) to 31.5 °C (**figure 6B**).

492

493 *4.2.2 U-Guan⁺ Receptor Binding Affinity*



494

495

496 **Figure 7: U-Guan⁺-phosphate normalized PO₂⁻ stretch at 5.5 °C (A) and 31.5 °C (B)**

497 **showing an increase in intensity with phosphate addition until binding site saturation.**

498

499 The K_a for phosphate binding to U-Guan⁺ was again quantified using the general

500 Langmuir fit by integrating the phosphate PO₂⁻ stretch (**figure 7**). To account for the temperature

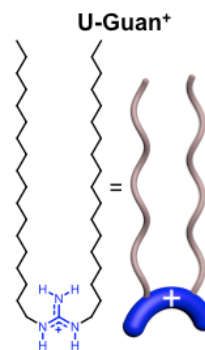
501 effect, the more narrow peak of the 5.5 °C spectra were integrated from 1019-1200 cm⁻¹ (**figure**

502 7A), and the more broad 31.5 °C peak from 992-1200 cm⁻¹ (**figure 7B**). The integration of each
 503 PO₂⁻ peak again had the spectral intensity of water subtracted and were normalized to the
 504 maximum intensity. The error associated with the averaging of three spectra per phosphate
 505 concentration was propagated through the subtraction of water intensity and the division of the
 506 maximum intensity normalization. The value of K_a for **U-Guan⁺**-phosphate binding at 5.5 °C
 507 and 31.5 °C was determined to be 1.3×10⁶ ± 0.7×10⁶ M⁻¹ and 2.3×10⁵ ± 1×10⁵ M⁻¹ respectively.
 508 The magnitude of K_a is again higher at the lower temperature suggesting an enthalpically driven
 509 binding process. At the higher temperature the receptor does not bind phosphate as well due to
 510 the excess thermal energy present in the system.

511

512 *4.2.3 Thermodynamic Driving Forces of U-Guan⁺-phosphate Binding*

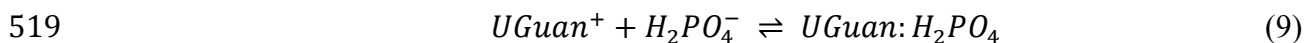
T	K (M ⁻¹)	1/T	ln K	error
278.5 K	1.29×10 ⁶	0.00359	14.069	±0.55
304.5 K	2.26×10 ⁵	0.00328	12.329	±0.68



513 **Figure 8: U-Guan⁺ Van't Hoff data from which the ΔH^o_b and the ΔS^o_b were respectively**
 514 **obtained.**

516

517 Assuming 1:1 binding for the **U-Guan**⁺ receptor to phosphate, the K_a for binding may be
518 modeled as a chemical equilibrium between bound and unbound states (equations 9,10).



520
$$K_a = \frac{(UGuan:H_2PO_4)}{(UGuan^+)(H_2PO_4^{2-})} \quad (8)$$

521 As seen with the **U-Ammo**⁺ receptor the K_a for **U-Guan**⁺ binding at both low and high
522 temperatures are of large magnitude therefore suggesting that the equilibrium lies heavily to the
523 right, favoring the bound state over the unbound state. The slope of a line may be approximated
524 from the two points in **figure 8**, and used with the Van't Hoff equations (equations 2-6) to obtain
525 ΔS_b from the y-intercept and ΔH_b from the slope of the line. As before, a third data point at 15
526 °C will be obtained to confirm the equation of the line used herein. The ΔG_b may then be
527 obtained at each temperature, the summary of which may be seen in **Table 2**.

528

U-Guan⁺					
$K_{a,5.5^\circ C}$ (M^{-1})	$K_{a,31.5^\circ C}$ (M^{-1})	ΔH_b (J/mol)	ΔS_b (J/mol K)	$\Delta G_{5.5^\circ C}$ (J/mol)	$\Delta G_{31.5^\circ C}$ (J/mol)
1.3×10 ⁶	2.3×10 ⁵	-685	-0.763	-472.0	-452.3

529 **Table 2: Thermodynamic values for U-Guan⁺-phosphate binding**

530

531 This binding system is also enthalpically driven and entropically hindered as observed in the **U-**
532 **Ammo**⁺ binding system. The unfavorable negative ΔS_b may be attributed to the rearrangement
533 that must occur upon the phosphate binding to the receptor in the monolayer – transitioning from
534 a less ordered and unbound system to a more ordered and bound system. However once again the
535 favorable negative ΔH_b drives the binding and is created by the low ϵ of the air – water interface,

536 thus allowing for electrostatic and hydrogen bond attractions between the guanidinium and
537 phosphate to proceed unhindered.

538

539 4.3 Comparison of U-Ammo⁺ and U-Guan⁺ Affinity for Phosphate

540

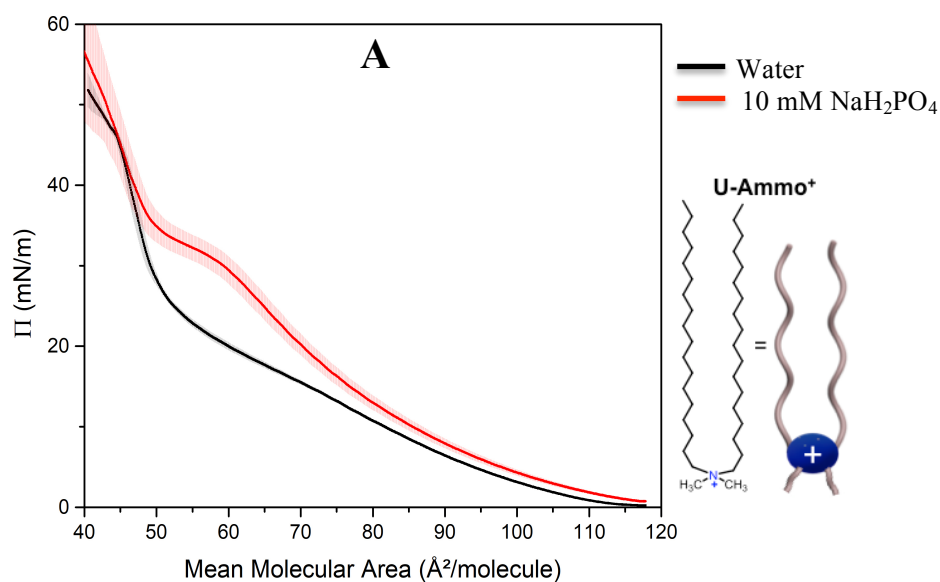
	$K_a, 5.5^\circ \text{C}$ (M^{-1})	$K_a, 31.5^\circ \text{C}$ (M^{-1})	ΔH_b (J/mol)	ΔS_b (J/molK)	$\Delta G_{5.5^\circ \text{C}}$ (J/mol)	$\Delta G_{31.5^\circ \text{C}}$ (J/mol)
U-Ammo⁺	3.62×10^5	5.9×10^3	-1621	-4.27	-429.2	-318.2
U-Guan⁺	1.3×10^6	2.3×10^5	-685	-0.763	-472.0	-452.3

541 **Table 3: Summary of Thermodynamic Data for U-Ammo⁺ and U-Guan⁺ Receptors**

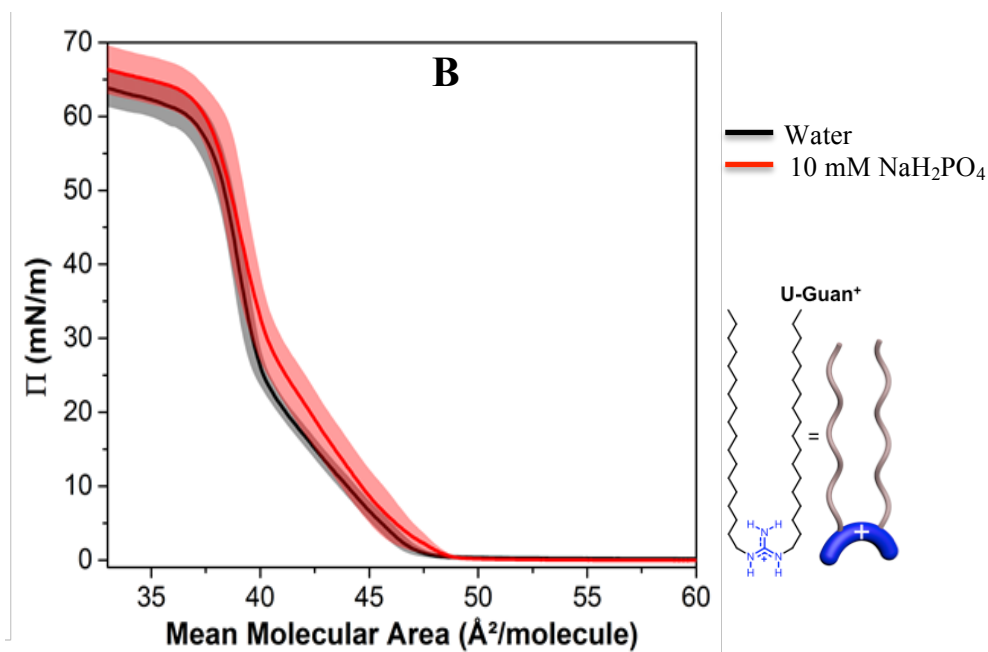
542

543 The thermodynamic quantities for phosphate binding may be compared (**table 3**) in order
544 to propose which receptor is energetically more favorable to sequester phosphate at the air –
545 water interface. A comparison of receptor K_a magnitudes can give the first insight that **U-Guan⁺**
546 is the better phosphate receptor. The magnitudes of K_a for **U-Guan⁺** are at least one order of
547 magnitude larger than **U-Ammo⁺** at both high and low temperature. In comparing the enthalpic
548 driving forces, both receptors have negative ΔH_b indicating enthalpy is the main driving force,
549 however it may be seen that **U-Ammo⁺** has the larger enthalpic driving force. One way that this
550 may be explained, through electrostatic attraction, is that the positive charge on the guanidinium
551 head group is delocalized between three nitrogen constituents of the functional group via
552 resonance. This charge delocalization may act to slightly decrease the electrostatic potential of
553 the group, creating a smaller electrostatic potential difference between H_2PO_4^- and **U-Guan⁺**. In
554 contrast the positive charge on the ammonium head group is not delocalized via resonance

555 suggesting a larger electrostatic potential difference between H_2PO_4^- and U-Ammo^+ - giving rise
556 to more enthalpically favored binding.



557

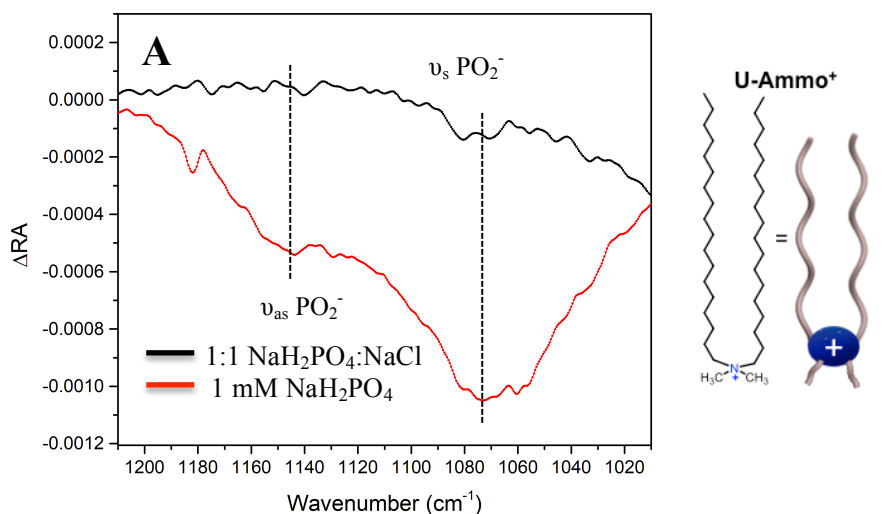


558
559 **Figure 9: Π -A isotherms on water and 10 mM phosphate at 21 °C for U-Ammo^+ (A) and U-
560 Guan^+ (B, from Neal 2019 *et. al* in review) with shaded regions representing one standard
561 deviation above and below the average of three trials.**

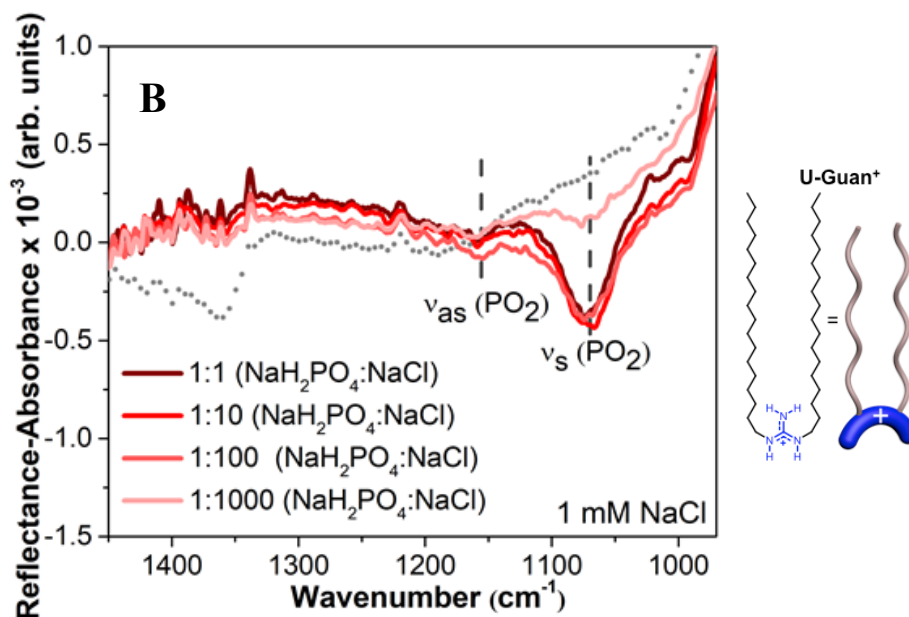
562

563 In analysis of ΔS_b it may be seen that binding in this unique environment is entropically
564 unfavorable for both receptors. However ΔS_b for **U-Guan⁺** is less negative than for **U-Ammono⁺**
565 suggesting that entropic hindrance is less of a barrier for the former binding than the latter. This
566 may be explained via a discussion of the organization of the Langmuir monolayer and visualized
567 using the Π -A isotherms of both receptors on water and phosphate subphases (**figure 9**). The
568 isotherms of **U-Ammono⁺** on 10 mM phosphate show a large expansion in mean molecular area
569 from the isotherm on water (**figure 9A**). This is contrasted by the isotherms of **U-Guan⁺** on
570 water and phosphate (from Neal *et. al* 2019, in review), which show minimal expansion (**figure**
571 **9B**). An increase in mean molecular area upon phosphate binding to **U-Ammono⁺** suggests that the
572 monolayer had to reorganize and reorient in order to bind phosphate. This reorganization may be
573 a product of the bulky methyl groups at the ammonium head group, thus resulting in a larger
574 entropic barrier to phosphate binding. The **U-Guan⁺** shows minimal expansion upon phosphate
575 binding, suggesting that the monolayer did not have to reorganize. The preorganization of the
576 guanidinium group with the hydrogen bond donors has been taken advantage of before for
577 phosphate capture^{16,24,25,50} - a property that is observed here as well. A lack of the need for
578 monolayer reorganization and reorientation and the presence of hydrogen bond donors for
579 phosphate binding to **U-Guan⁺** suggest that this receptor has a lower entropic barrier, which is
580 experimentally supported by the less negative magnitude of ΔS_b . In comparing the values for
581 $\Delta G_{b,T}$ it may be seen that enthalpic driving force of **U-Guan⁺** electrostatic binding coupled with
582 the lower entropic barrier of binding due to organization and hydrogen bond donors in the
583 guanidinium group result in **U-Guan⁺** having more negative $\Delta G_{b,T}$ overall than **U-Ammono⁺**. A
584 more negative $\Delta G_{b,T}$ suggests that **U-Guan⁺** is a better phosphate receptor than **U-Ammono⁺**.
585

586 **4.4 Anion Selectivity of Receptors Between Chloride and Phosphate Anions**



587



588

589 **Figure 10: U-Ammo⁺ on 1 mM phosphate to 1 mM chloride IRRAS compared to 1 mM**
 590 **phosphate IRRAS showing a decrease in PO₂⁻ stretching intensity with chloride addition**
 591 **(A) and U-Guan⁺ IRRAS on varying ratios of phosphate to chloride showing selectivity up**
 592 **to 1:1000 (B, from Neal 2019 *et. al* in review).**

593

594 The hydrogen bond-assisted electrostatics of the phosphate binding to **U-Guan**⁺ not only
595 make the receptor more energetically favorable, but also makes the receptor selective to
596 phosphate over other anions such as chloride in solution (**Figure 10**). **Figure 10A** shows that the
597 PO₂⁻ IRRAS stretch for **U-Ammono**⁺ has significantly decreased in intensity in a 1 mM chloride to
598 1 mM phosphate solution compared to a 1 mM phosphate solution in which the PO₂⁻ symmetric
599 and asymmetric bands are clearly visible. The decrease in intensity in the 1:1 phosphate-chloride
600 solution suggests that **U-Ammono**⁺ is binding to chloride anions rather than phosphate anions. This
601 is likely the result of the pure electrostatics available for binding at the ammonium head group
602 preferring chloride, a smaller anion with a more localized negative charge, over H₂PO₄⁻, a larger
603 anion with a delocalized negative charge. The opposite is observed for **U-Guan**⁺ in a phosphate
604 selectivity study by Neal *et. al*, 2019 (in review) in which **U-Guan**⁺ shows selectivity for H₂PO₄⁻
605 over chloride even at 1:1000 ratios of phosphate to chloride sub-phase concentration (**Figure**
606 **10B**). The selectivity of **U-Guan**⁺ binding to phosphate is a product of the hydrogen bond-
607 assisted electrostatic interactions of this receptor preferentially binding to the hydrogen bond
608 acceptor sites on H₂PO₄⁻. The high phosphate selectivity suggests that **U-Guan**⁺ is a better
609 phosphate receptor than **U-Ammono**⁺ in an aqueous environment with both chloride and phosphate
610 anions.

611

612

613 **CHAPTER 5: CONCLUSIONS AND FUTURE WORK**

614 There is a growing need to understand the principles and driving forces of aqueous
615 phosphate capture. Phosphorus is integral to water management, energy conservation, and food
616 security. With limited supplies of phosphorus rock and a growing demand for fertilizers to feed

617 an increasing world population there is a need to capture and recycle anthropogenic phosphate
618 that is lost to water sources through agricultural runoff. Additionally, the eutrophication ignited
619 by phosphate in water sources is a growing environmental danger and in need of remediation. In
620 order to close the human phosphorus cycle, the principles and challenges of phosphate
621 recognition must be understood and overcome. Studying phosphate capture at the air – water
622 interface via Langmuir monolayers provides benefits for binding studies. Two amphiphilic
623 molecules **U-Ammo⁺** and **U-Guan⁺** were studied at the interface via IRRAS to determine the
624 driving forces of phosphate capture and to compare a pure electrostatic binding receptor, **U-**
625 **Ammo⁺**, to a hydrogen bond-assisted electrostatic binding receptor, **U-Guan⁺**. Association
626 binding constants for these two molecules were determined at 5.5 °C and 31.5 °C via a general
627 Langmuir fit. Van't Hoff analysis then allowed the enthalpy of binding and entropy of binding to
628 be determined for both molecules, which allowed quantification of the free energy of binding at
629 low and high temperature. The **U-Guan⁺** receptor proved a thermodynamically better phosphate
630 receptor than **U-Ammo⁺** due to the overall larger binding constants and more negative free
631 energy driving force. Additionally, the phosphate selectivity of both receptors were qualitatively
632 determined based upon IRRAS. It was shown that the **U-Ammo⁺** receptor was not selective to
633 phosphate at 1:1 phosphate to chloride aqueous concentrations, and a previous study showed that
634 **U-Guan⁺** is selective to phosphate over chloride up to 1:1000 H₂PO₄⁻ to Cl⁻ ratios. This suggests
635 that the **U-Guan⁺** receptor is also a better phosphate recognition receptor due to its ability to
636 selectively bind phosphate via hydrogen bond-assisted electrostatic interactions. Future work for
637 this project that is required includes collecting more thermodynamic data to gain more
638 confidence in the results presented herein. The implications of these results are a contribution to

639 the understanding the principles of phosphate recognition for the further development of better
640 phosphate receptors.

641

642 **CHAPTER 6: REFERENCES**

- 643 (1) Jarvie, H. P.; Sharpley, A. N.; Flaten, D.; Kleinman, P. J.; Jenkins, A.; Simmons, T. The
644 Pivotal Role of Phosphorus in a Resilient Water–Energy–Food Security Nexus. *J.*
645 *Environ. Qual.* **2015**, *44* (4).
- 646 (2) Cordell, D.; Drangert, J. O.; White, S. The Story of Phosphorus: Global Food Security and
647 Food for Thought. *Glob. Environ. Chang.* **2009**, *19* (2) 292-305.
- 648 (3) Deliomeroğlu, M. K.; Lynch, V. M.; Sessler, J. L. Conformationally Switchable Non-
649 Cyclic Tetrapyrrole Receptors: Synthesis of Tetrakis(1H-Pyrrole-2-Carbaldehyde)
650 Derivatives and Their Anion Binding Properties. *Chem. Commun.* **2014**, *50*(80), 11863–
651 11866.
- 652 (4) Springmann, M.; Clark, M.; Mason-D’Croz, D.; Wiebe, K.; Bodirsky, B. L.; Lassaletta,
653 L.; de Vries, W.; Vermeulen, S. J.; Herrero, M.; Carlson, K. M.; et al. Options for Keeping
654 the Food System within Environmental Limits. *Nature* **2018**, *562*(7728), 519–525.
- 655 (5) Elrashidi, M. A.; Mays, M. D.; Harder, J.; Schroeder, D.; Brakhage, P. Loss of
656 Phosphorus by Runoff For Agricultural Watersheds. *Soil Sci.* **2005**, *170* (7), 543–558.
- 657 (6) Sims, J. T.; Simard, R. R.; Joern, B. C. Phosphorus Loss in Agricultural Drainage:
658 Historical Perspective and Current Research. *J. Environ. Qual.* **2010**, *27*(2), 277.
- 659 (7) Ryther, J. H.; Dunstan, W. M. Nitrogen, Phosphorus, and Eutrophication in the Coastal
660 Marine Environment 1008-1013. *Science* . **1971**, *171*(3975), 1008–1013.
- 661 (8) Sharpley, A. N.; Chapra, S. C.; Wedepohl, R.; Sims, J.; Daniel, T. C.; Reddy, K. R.

- 662 Managing Agricultural Phosphorous for Protection of Surface Waters: Issues and Options.
663 *J. Environ. Qual.* **1994**, 23(3), 437
- 664 (9) Conley, D. J.; Paerl, H. W.; Howarth, R. W.; Boesch, D. F.; Seitzinger, S. P.; Havens, K.
665 E.; Lancelot, C.; Likens, G. E. Ecology - Controlling Eutrophication: Nitrogen and
666 Phosphorus. *Science*. 2009.
- 667 (10) Correll, D. L. The Role of Phosphorus in the Eutrophication of Receiving Waters: A
668 Review. *J. Environ. Qual.* **2010**.
- 669 (11) Elrashidi, M. A.; Mays, M. D.; Fares, A.; Seybold, C. A.; Harder, J. L.; Peaslee, S. D.;
670 VanNeste, P. Loss of Nitrate-Nitrogen by Runoff and Leaching for Agricultural
671 Watersheds. *Soil Sci.* **2005**.
- 672 (12) Elrashidi, M. A.; Mays, M. D.; Peaslee, S. D.; Hooper, D. G. A Technique to Estimate
673 Nitrate-Nitrogen Loss by Runoff and Leaching for Agricultural Land, Lancaster County,
674 Nebraska. *Commun. Soil Sci. Plant Anal.* **2004**.
- 675 (13) Minch, M. J. An Introduction to Hydrogen Bonding (Jeffrey, George A.). *J. Chem. Educ.*
676 **2009**.
- 677 (14) Lam, H.-M.; Coschigano, K. T.; Oliveira, I. C.; Melo-Oliveira, R.; Coruzzi, G. M.
678 Molecular-Genetics of Nitrogen Assimilation Into Amino Acids in Higher Plants. *Annu.*
679 *Rev. Plant Physiol. Plant Mol. Biol.* **1996**.
- 680 (15) Cremer, P. S.; Flood, A. H.; Gibb, B. C.; Mobley, D. L. Collaborative Routes to
681 Clarifying the Murky Waters of Aqueous Supramolecular Chemistry. *Nature Chemistry*.
682 2017.
- 683 (16) Hargrove, A. E.; Nieto, S.; Zhang, T.; Sessler, J. L.; Anslyn, E. V. Artificial Receptors for
684 the Recognition of Phosphorylated Molecules. *Chemical Reviews*. 2011.

- 685 (17) Wang, Z.; Luecke, H.; Yao, N.; Quioco, F. A. A Low Energy Short Hydrogen Bond in
686 Very High Resolution Structures of Protein Receptor-Phosphate Complexes. *Nat. Struct.*
687 *Biol.* **1997**.
- 688 (18) Neal, J. F.; Zhao, W.; Grooms, A. J.; Flood, A. H.; Allen, H. C. Arginine-Phosphate
689 Recognition Enhanced in Phospholipid Monolayers at Aqueous Interfaces. *J. Phys. Chem.*
690 *C* **2018**.
- 691 (19) Marcus, Y. Thermodynamics of Solvation of Ions. Part 5. - Gibbs Free Energy of
692 Hydration at 298.15 K. *J. Chem. Soc. Faraday Trans.* **1991**.
- 693 (20) Kubik, S. Anion Recognition in Water. *Chemical Society Reviews*. 2010.
- 694 (21) Fumagalli, L.; Esfandiari, A.; Fabregas, R.; Hu, S.; Ares, P.; Janardanan, A.; Yang, Q.;
695 Radha, B.; Taniguchi, T.; Watanabe, K.; et al. Anomalously Low Dielectric Constant of
696 Confined Water. *Science (80-.)*. **2018**.
- 697 (22) Ariga, K.; Tamagawa, H.; Inoue, Y.; Kunitake, T.; Sakurai, M. Theoretical Study of
698 Intermolecular Interaction at the Lipid–Water Interface. 2. Analysis Based on the
699 Poisson–Boltzmann Equation. *J. Phys. Chem. B* **2002**.
- 700 (23) Rumble, J. R. ed. Handbook of Chemistry and Physics 99th Edition.
- 701 (24) Sasaki, D. Y.; Kurihara, K.; Kunitake, T. Specific, Multiple-Point Binding of ATP and
702 AMP to a Guanidinium-Functionalized Monolayer. *Journal of the American Chemical*
703 *Society*. 1991.
- 704 (25) Dietrich, B.; Hosseini, M. W.; Lehn, J. M.; Sessions, R. B. Anion Receptor Molecules.
705 Synthesis and Anion-Binding Properties of Polyammonium Macrocycles. *J. Am. Chem.*
706 *Soc.* **1981**.
- 707 (26) Ariga, K.; Anslyn, E. V. Manipulating the Stoichiometry and Strength of Phosphodiester

- 708 Binding to a Bisguanidine Cleft in DMSO/Water Solutions. *J. Org. Chem.* **1992**.
- 709 (27) Kneeland, D. M.; Ariga, K.; Lynch, V. M.; Huang, C. Y.; Anslyn, E. V.
- 710 Bis(Alkylguanidinium) Receptors for Phosphodiesteres: Effect of Counterions, Solvent
- 711 Mixtures, and Cavity Flexibility on Complexation. *J. Am. Chem. Soc.* **1993**.
- 712 (28) Dixon, R. P.; Geib, S. J.; Hamilton, A. D. Molecular Recognition: Bis-Acylguanidiniums
- 713 Provide a Simple Family of Receptors for Phosphodiesteres. *J. Am. Chem. Soc.* **1992**.
- 714 (29) Kalinin, S. V. Feel the Dielectric Force. *Science (80-.)*. **2018**.
- 715 (30) Liu, Y.; Sengupta, A.; Raghavachari, K.; Flood, A. H. Anion Binding in Solution: Beyond
- 716 the Electrostatic Regime. *Chem* **2017**.
- 717 (31) Israelachvili, J. N.; Pashley, R. M. Molecular Layering of Water at Surfaces and Origin of
- 718 Repulsive Hydration Forces. *Nature* **1983**.
- 719 (32) Toney, M. F.; Howard, J. N.; Richer, J.; Borges, G. L.; Gordon, J. G.; Melroy, O. R.;
- 720 Wiesler, D. G.; Yee, D.; Sorensen, L. B. Voltage-Dependent Ordering of Water Molecules
- 721 at an Electrode-Electrolyte Interface. *Nature* **1994**.
- 722 (33) Velasco-Velez, J. J.; Wu, C. H.; Pascal, T. A.; Wan, L. F.; Guo, J.; Prendergast, D.;
- 723 Salmeron, M. The Structure of Interfacial Water on Gold Electrodes Studied by X-Ray
- 724 Absorption Spectroscopy. *Science (80-.)*. **2014**.
- 725 (34) Lee, I. C.; Frank, C. W.; Yamamoto, T.; Tseng, H. R.; Flood, A. H.; Stoddart, J. F.;
- 726 Jeppesen, J. O. Langmuir and Langmuir-Blodgett Films of Amphiphilic Bistable
- 727 Rotaxanes. *Langmuir* **2004**.
- 728 (35) Jang, S. S.; Jang, Y. H.; Kim, Y. H.; Goddard, W. A.; Choi, J. W.; Heath, J. R.; Laursen,
- 729 B. W.; Flood, A. H.; Stoddart, J. F.; Nørgaard, K.; et al. Molecular Dynamics Simulation
- 730 of Amphiphilic Bistable [2]Rotaxane Langmuir Monolayers at the Air/Water Interface. *J.*

- 731 *Am. Chem. Soc.* **2005**.
- 732 (36) Cram, D. J. The Design of Molecular Hosts, Guests, and Their Complexes (Nobel
733 Lecture). *Angewandte Chemie International Edition in English*. 1988.
- 734 (37) Schmidtchen, F. P.; Berger, M. Artificial Organic Host Molecules for Anions. *Chem. Rev.*
735 **1997**.
- 736 (38) Onda, M.; Yoshihara, K.; Koyano, H.; Ariga, K.; Kunitake, T. Molecular Recognition of
737 Nucleotides by the Guanidinium Unit at the Surface of Aqueous Micelles and Bilayers. A
738 Comparison of Microscopic and Macroscopic Interfaces. *J. Am. Chem. Soc.* **1996**.
- 739 (39) Tohda, K.; Amemiya, S.; Ohki, T.; Nagahora, S.; Tanaka, S.; Bühlmann, P.; Umezawa, Y.
740 Channel Mimetic Sensing Membranes for Nucleotides Based on Multitopic Hydrogen
741 Bonding. *Isr. J. Chem.* **1997**.
- 742 (40) Beer, P. D.; Davis, J. J.; Drillsma-Milgrom, D. A.; Szemes, F. Anion Recognition and
743 Redox Sensing Amplification by Self-Assembled Monolayers of 1,1'-Bis(Alkyl-N-
744 Amido)Ferrocene. *Chem. Commun.* **2002**.
- 745 (41) Turygin, D. S.; Subat, M.; Raitman, O. A.; Selector, S. L.; Arslanov, V. V.; König, B.;
746 Kalinina, M. A. Two-Dimensional Arrays of Amphiphilic Zn²⁺-Cyclens for Guided
747 Molecular Recognition at Interfaces. *Langmuir* **2007**.
- 748 (42) Sovago, M.; Wurpel, G. W. H.; Smits, M.; Müller, M.; Bonn, M. Calcium-Induced
749 Phospholipid Ordering Depends on Surface Pressure. *J. Am. Chem. Soc.* **2007**.
- 750 (43) Badis, M.; Tomaszewicz, I.; Joly, J. P.; Rogalska, E. Enantiomeric Recognition of
751 Amino Acids by Amphiphilic Crown Ethers in Langmuir Monolayers. *Langmuir* **2004**.
- 752 (44) Blankenburg, R.; Meller, P.; Ringsdorf, H.; Salesse, C. Interaction between Biotin Lipids
753 and Streptavidin in Monolayers: Formation of Oriented Two-Dimensional Protein

- 754 Domains Induced by Surface Recognition. *Biochemistry* **1989**.
- 755 (45) Mendelsohn, R. External Infrared Reflection Absorption Spectrometry of Monolayer
756 Films at the Air-Water Interface. *Annu. Rev. Phys. Chem.* **2002**.
- 757 (46) Thomas, L. C.; Chittenden, R. A. Characteristic Infrared Absorption Frequencies of
758 Organophosphorus Compounds—I The Phosphoryl (P=O) Group. *Spectrochim. Acta*
759 **2002**.
- 760 (47) Thomas, L. C.; Chittenden, R. A. Characteristic Infrared Absorption Frequencies of
761 Organophosphorus Compounds-VII. Phosphorus Ions. *Spectrochim. Acta Part A Mol.*
762 *Spectrosc.* **1970**.
- 763 (48) Rudolph, W. W. Raman- and Infrared-Spectroscopic Investigations of Dilute Aqueous
764 Phosphoric Acid Solutions. *Dalt. Trans.* **2010**.
- 765 (49) Ma, G.; Allen, H. C. DPPC Langmuir Monolayer at the Air-Water Interface: Probing the
766 Tail and Head Groups by Vibrational Sum Frequency Generation Spectroscopy. *Langmuir*
767 **2006**.
- 768 (50) Xiao, K. P.; Buhlmann, P.; Umezawa, Y. Ion-Channel-Mimetic Sensing of Hydrophilic
769 Anions Based on Monolayers of a Hydrogen Bond-Forming Receptor. *Anal. Chem.* **1999**.
- 770 (51) Masayuki, D. Y.; Yanagi, M.; Kurihara, K.; Kunitake, T. The Interaction of a
771 Guanidinium Monolayer with ATP and AMP, as Revealed by Surface Potential and UV
772 Absorption Measurements. *Thin Solid Films* **1992**.
- 773 (52) Blondeau, P.; Segura, M.; Pérez-Fernández, R.; De Mendoza, J. Molecular Recognition of
774 Oxoanions Based on Guanidinium Receptors. *Chem. Soc. Rev.* **2007**.
- 775 (53) Schug, K. A.; Lindner, W. Noncovalent Binding between Guanidinium and Anionic
776 Groups: Focus on Biological- and Synthetic-Based Arginine/Guanidinium Interactions

- 777 with Phosph[on]Ate and Sulf[on]Ate Residues. *Chem. Rev.* **2005**.
- 778 (54) Tobey, S. L.; Anslyn, E. V. Energetics of Phosphate Binding to Ammonium and
779 Guanidinium Containing Metallo-Receptors in Water. *J. Am. Chem. Soc.* **2003**.
- 780 (55) Linton, B.; Hamilton, A. D. Calorimetric Investigation of Guanidinium-Carboxylate
781 Interactions. *Tetrahedron* **1999**.
- 782 (56) Berger, M.; Schmidtchen, F. P. The Binding of Sulfate Anions by Guanidinium Receptors
783 Is Entropy-Driven. *Angew. Chemie - Int. Ed.* **1998**.
- 784 (57) Elsiddig, R.; Hughes, H.; Owens, E.; O'Reilly, N. J.; O'Grady, D.; McLoughlin, P.
785 Kinetic and Thermodynamic Evaluation of Phosphate Ions Binding onto Sevelamer
786 Hydrochloride. *Int. J. Pharm.* **2014**.
- 787 (58) Engel, T.; Reid, P. *Thermodynamics, Statistical Thermodynamics, & Kinetics*, Second
788 Edi.; Kaveney, D., DuPont, C., Eds.; Pearson Education, 2010.
- 789 (59) Sharma, G.; First, E. A. Thermodynamic Analysis Reveals a Temperature-Dependent
790 Change in the Catalytic Mechanism of Bacillus Stearothermophilus Tyrosyl-TRNA
791 Synthetase. *J. Biol. Chem.* **2009**.
- 792 (60) Casillas-Ituarte, N. N.; Chen, X.; Castada, H.; Allen, H. C. Na⁺ and Ca²⁺ Effect on the
793 Hydration and Orientation of the Phosphate Group of DPPC at Air - Water and Air -
794 Hydrated Silica Interfaces. *J. Phys. Chem. B* **2010**.
- 795 (61) Chapman, A. C.; Thirlwell, L. E. Spectra of Phosphorus Compounds—I the Infra-Red
796 Spectra of Orthophosphates. *Spectrochim. Acta* **2002**.
- 797 (62) Klähn, M.; Mathias, G.; Kötting, C.; Nonella, M.; Schlitter, J.; Gerwert, K.; Tavan, P. IR
798 Spectra of Phosphate Ions in Aqueous Solution: Predictions of a DFT/MM Approach
799 Compared with Observations. *J. Phys. Chem. A* **2004**.

